WAVE AND SEDIMENT DYNAMICS AT SHELLY BEACH

Numerical modelling of sediment transport due to waves and tidal currents and an investigation of the efficacy of the Long Mac to maintain beach stability

Prepared for Port Otago Limited

PO Box 441, New Plymouth, New Zealand
T: 64-6-7585035 E: enquiries@metocean.co.nz

MetOcean Solutions Ltd: P0140-01

June 2013

Report status

Version	Date	Status	Approved by
RevA	15/06/2013	Interim draft for internal review	Weppe
RevB	16/06/2013	Interim draft for client review	McComb
Rev0	28/08/2014	Approved for release	McComb

It is the responsibility of the reader to verify the currency of the version number of this report.

PO Box 441, New Plymouth, New Zealand
T: 64-6-7585035 E: enquiries@metocean.co.nz

TABLE OF CONTENTS

LIST OF FIGURES

LIST OF TABLES

1. INTRODUCTION

A requirement of consent for Port Otago's channel deepening consent was research into the function of the "Long Mac" groyne, which is immediately adjacent to this shipping channel, opposite Harington Point.

One of the current dredge spoil disposal grounds is located just offshore of Shelly Beach which is partially bounded to the east by the submerged groyne commonly referred to as "Long Mac". This structure and other groynes and rock structures on the eastern side of the channel were implemented between 1905 and 1910 to help stabilise the beach, prevent direct sediment recirculation back into the channel and hold the alignment of the main shipping channel. However, the state of this structure has degraded over time and the efficacy of its function in stabilising the beach has been called into question.

As a first step in addressing the issue, a study has been commissioned to investigate the wave and sediment transport dynamics in this highly complex area, with particular attention to the functional aspects of the local features and the potential for sediment recirculation into the channel and Harbour. A numerical model of the area has been implemented to characterize the local sediment morphodynamics and the effect of the Long Mac – both in its current form and in an optimised configuration.

The study region necessarily incudes the wider Otago Harbour entrance region (Figure 1.1). This captures the large submerged ebb delta bar east of the shipping channel, Shelly Beach, enclosed by the Mole to the west and the Long Mac to the east, and the bend of the channel south of Shelly Beach known as "Harrington Bend". In the following text the harbour "entrance" refers to this area.

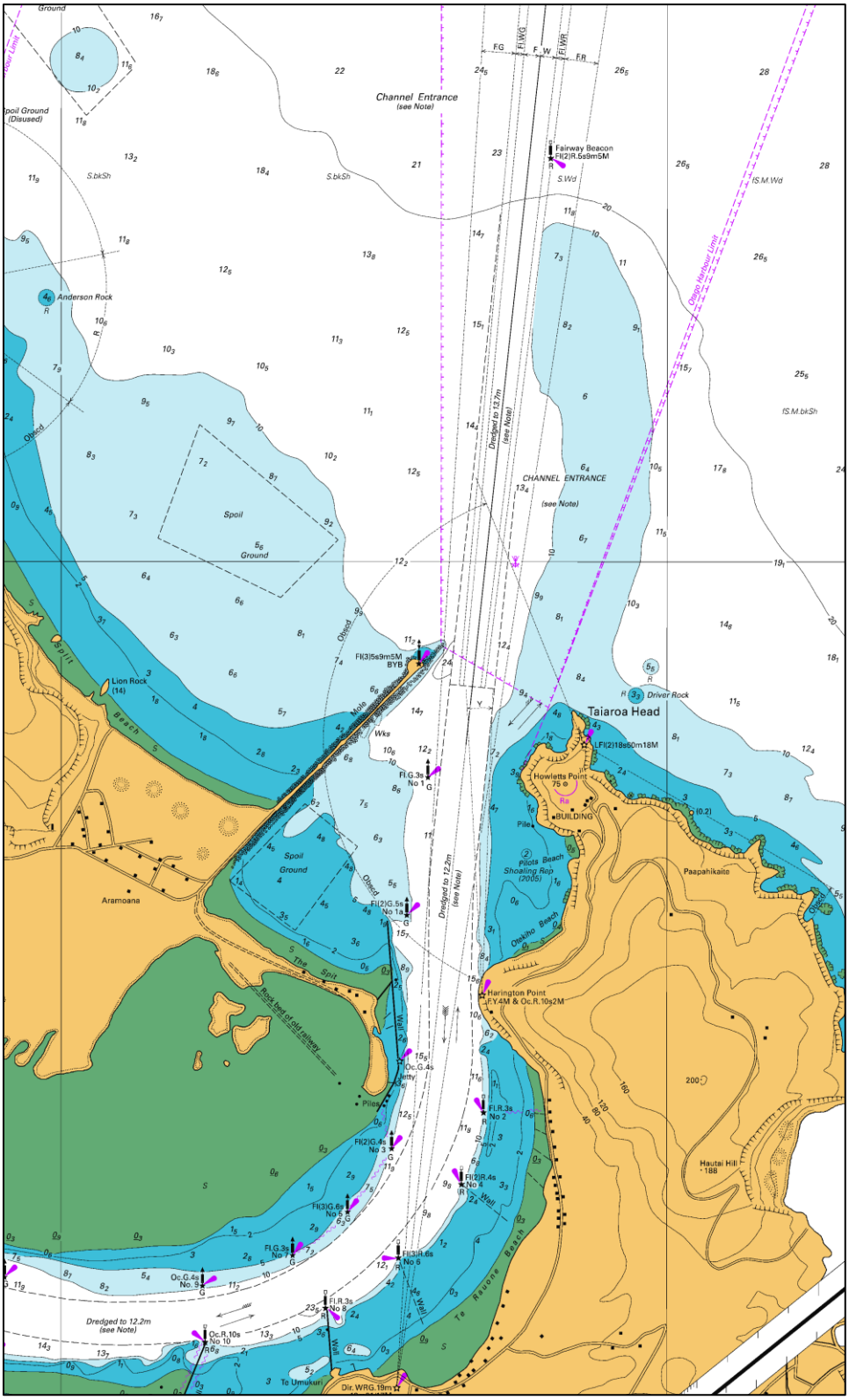

Figure 1.1 Nautical chart of the study area including the submerged ebb delta bar, Shelly Beach, the Mole and Long Mac.

2. NUMERICAL MODELLING METHODOLOGY

The numerical modelling approach included the use of a regional hydrodynamic model covering the whole Otago Harbour and Peninsula eastern and northern coasts, and a local high-resolution morphodynamic model focusing on the entrance region and coupling flow, wave and sediment transport models. The regional hydrodynamic model was required to ensure correct representation of the complex tidal dynamics developing in the entrance region due to the coupling of the Harbour with the larger scale regional tidal regime, and allowed nesting of the high resolution domain.

2.1. Regional tidal hydrodynamic modelling (SELFE)

SELFE is a prognostic finite-element unstructured-grid model designed to simulate 3D baroclinic, 3D barotropic or 2D barotropic circulation. The barotropic mode equations employ a semi-implicit finite-element Eulerian-Lagrangian algorithm to solve the shallow-water equations, forced by relevant physical processes (atmospheric, oceanic and fluvial forcing). SELFE uses either pure terrain-following sigma, or S-layer coordinates in the vertical, or a hybrid system using both S and Z-layers as required and uses sophisticated vertical turbulent closure models. A detailed description of the SELFE model formulation, governing equations and numerics can be found in Zhang and Baptista (2008). For the purposes of this study, SELFE was run in full 3D barotropic mode, with tidal velocity fields at each sigma level.

2.1.1. Model domain

The model domain is shown on Figure 2.1. It includes the entire Otago Harbour and a wide stretch of the Otago coast, from Wickliffe Bay to the east to Karitane to the north, and extends ~ 10km offshore to depths of about 80 meters. The finite element mesh was refined in shallow regions and around complex features. The vertical discretization used 10 sigma levels with 30, 0.7 and 10 as the hc, θb and θf constants in the Song and Haidvogel's (1994) S-coordinate system.

2.1.2. Subgrid parameterisations

Vertical mixing was modelled using a k-kl model with a Kantha & Clayson (1994) stability function. A minimum and maximum diffusivity is applied, set to 1x10e-5 and 1x10e-1 m^2/s respectively. A constant surface mixing length of 0.1 m was used throughout. Frictional stress at the seabed was approximated with a quadratic drag law, with the drag coefficient (CD) determined using a bottom roughness of 0.001 m and an upper limit of CD set to 0.01.

2.1.3. Boundary and initial conditions

The SELFE grid was nested within the MetOcean Solutions Ltd. New Zealand tidal model which was run using an implementation of POM (Princeton Ocean Model). Both tidal surface elevation and current velocity were prescribed along the hemispheric (open) boundary. No residual currents were considered.

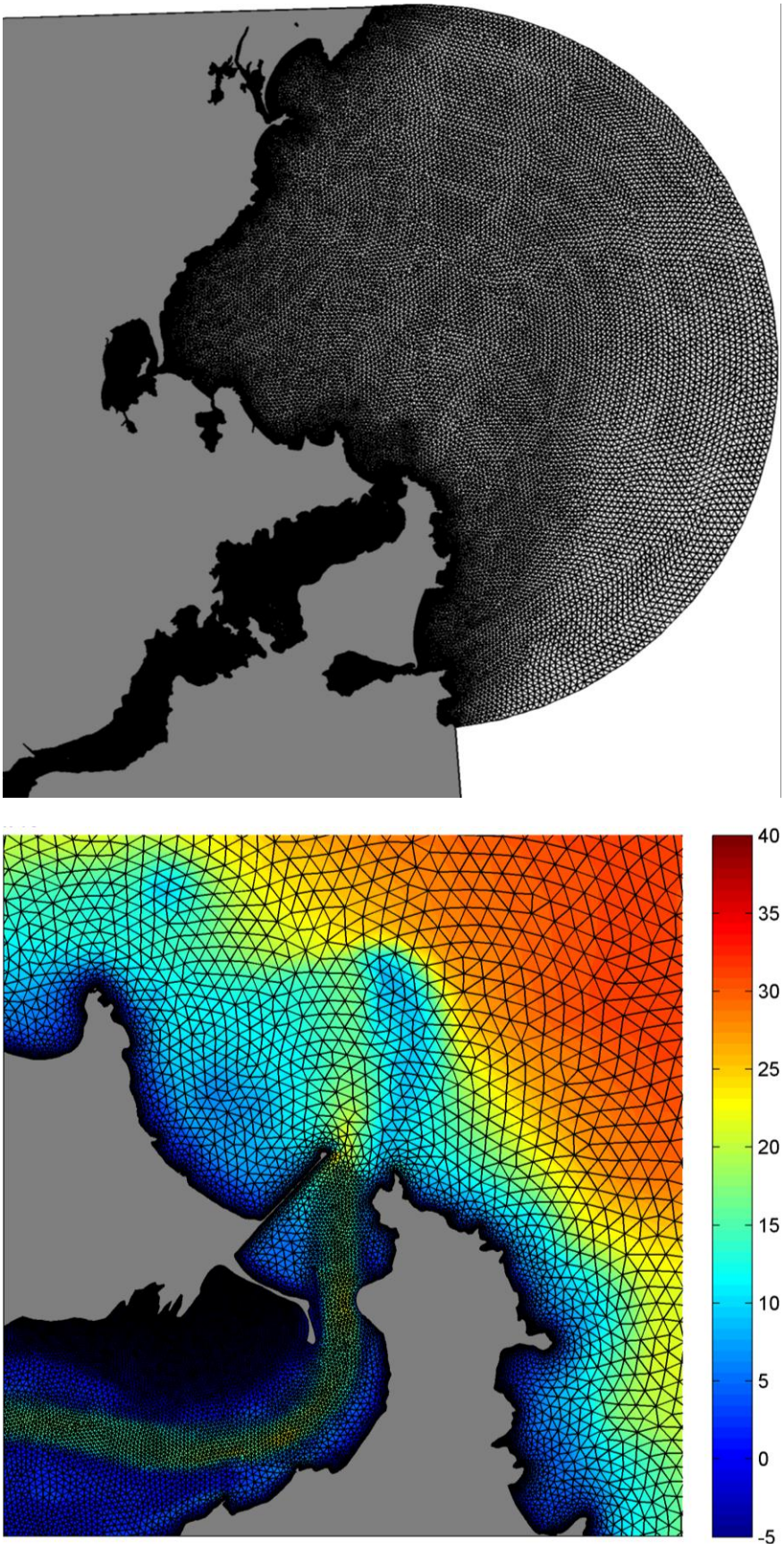

Figure 2.1 The hemispheric SELFE model domain (upper) and a zoomed in view of the entrance region with bathymetry (lower).

2.2. Local hydrodynamics, waves and sediment transport modelling (DELFT3D)

The Delft3D numerical model system (Lesser et al., 2004) was used to carry out the numerical simulations of coupled wave, current and sediment transport. The modelling system consists in three modules:

- Delft3D-WAVE is a nearshore wave propagation model which simulates the evolution of the incoming wave field.
- Delft3D-FLOW is a multi-dimensional (2D or 3D) hydrodynamic model which calculates non-steady flows and transport phenomena that result from tidal, meteorological and wave forcing.
- Delft3D-MOR computes the sediment transport fluxes and the resulting morphodynamic evolution based on the combined action of currents and waves.

The three modules are fully coupled to simulate the morphodynamic feedbacks. Every coupling time step, a new flow field (depth-averaged currents and water levels) is supplied from the hydrodynamic module to the wave module. The wave module propagates waves within the domain, accounting for the ambient hydrodynamics, and in turn provides radiation stress fields and basic wave parameters that will be used as forcing by the hydrodynamic module. Delft3D-MOR computes sediment transport based on the combined wave and current action, and updates the seabed morphology, thus affecting subsequent wave and flow computations.

Note that the updating of the seabed morphology can be switched off. In that case, the sediment transport fluxes are computed, but the model bathymetry is left unchanged. This is a useful option for studying general sediment transport pathways, without the unrealistic divergence that can occur due to uncorrected non-linear feedbacks between waves, currents and morphology. At this stage of the study, the model was run in non-updating mode to investigate the main sediment transport patterns in the entrance region and in the vicinity of the Long Mac.

2.2.1. Delft3D-WAVE

The third-generation SWAN model (Simulating WAves Nearshore) is used as the wave module (Holthuijsen et al., 2007). SWAN computes the evolution of random, short-crested waves in coastal regions with deep, intermediate and shallow water depths. The SWAN model accounts for (refractive) propagation due to depth and current and can represent the processes of wave generation by wind, dissipation due to white-capping, bottom friction and depth-induced wave breaking, and non-linear wave-wave interactions explicitly with state-of-the-art formulations (Deltares, 2013a).

For the present work, the local wave model boundary conditions are nested 2D spectral boundaries obtained from a regional scale grid forced by idealized wave events. This allows retaining the spatial variability of the incident wave field due to large scale regional refraction and sheltering effects. Bottom friction was modelled using the formulation of Collins (1972) and the default coefficient value of 0.015. Wave breaking was

modelled using a constant critical wave height to water depth ratio of 0.73 with a proportionality coefficient for the rate of dissipation of 1. No meteorological forcing was applied, so friction and wave breaking are the only dissipative mechanisms considered.

Since no updating of the seabed was considered, wave conditions were updated every 3 hours using the hydrodynamic field provided by the hydrodynamic module. This allowed saving some computational time while still representing variation of wave energy penetration due to tidal effects.

2.2.2. Delft3D-FLOW

The hydrodynamic module Delft3D-FLOW solves the Navier-Stokes equations for an uncompressible fluid under the shallow water and Boussinesq assumptions. The system of equations consists of the horizontal equations of motion, the continuity equation, the transport equations for conservative constituents, and a turbulence closure model. The details of equations and associated sub-models are fully described in Lesser et al.(2004) and the Delft3D-FLOW user manual (Deltares, 2013b)

The model was run in 2D mode, thus providing water levels and depth-averaged flows at each computational time step. Bed shear stresses are computed using a standard quadratic friction law using the bed roughness predictor of Van Rijn (2007) for the friction coefficients. The Van Rijn model allows prediction of time and spatially varying bed roughness based on basic hydrodynamic parameters and sediment characteristics. The non-linear enhancement of the bed shear stress in presence of waves was taken into account by means of the wave-current interaction model of Van Rijn et al. (2004). Turbulence effects are modelled using constant background horizontal and vertical eddy viscosity and eddy diffusivity coefficients. Horizontal background eddy viscosity and diffusivity are set equal to 5 m^2/s. A value of 10e-6 is used for the vertical background viscosity and diffusivity.

Water levels were prescribed at the northern (offshore side) and southern (harbour side) boundaries of the model domain, and so called “Neumann boundary conditions” were used on the cross-shore domain boundaries. Specifying cross-shore boundary condition can be problematic since a combination of processes will act throughout the model domain and may result in a water level and/or velocity distribution differing from that prescribed. Neumann boundaries let the model determine the correct solution at the boundaries imposing an alongshore water level gradient instead of a fixed water level or velocity (Roelvink and Walstra, 2006). Given the limited extents of the model domain, a uniform zero gradient was assumed along the domain lateral boundaries. The water levels prescribed at the model boundaries were generated from the regional scale (SELFE) tidal model, at half hourly interval. A time period covering several spring tidal cycles (16/04/2011 - 20/04/2011) was simulated to capture some of the most critical flows expected in the entrance region.

A time step of 3 seconds was used for the Delft3D-FLOW simulations, equivalent to maximum Courant numbers of approximately 8. The Courant number is a numerical stability criterion that needs to be less than 10 in Delft3D-FLOW (Deltares, 2013b).

2.2.3. Delft3D-MOR

The module Delft3D-MOR combines the information provided by the flow and wave modules to compute the sediment transport fluxes. The seabed level can then be updated as a result of the sediment sink and sources terms and computed transport gradients.

The updated expressions of Van Rijn, known as TRANSPOR2004 (Van Rijn, et al., 2004; Van Rijn, 2007a; Van Rijn, 2007b) were used to calculate the total sediment transport, including the bed load transport q_b and the suspended load transport q_s.

The bed load transport component consists of a current-related contribution (in the current direction), and a wave-related contribution (in the wave direction, following or opposing, depending on conditions). The suspended load transport includes a current-related contribution, due to advective processes (in the current direction) and the wave-related contribution, (in the wave direction, always onshore). Both wave contributions account for the wave asymmetry effects that develop as waves propagate in shallow waters due to non-linear processes.

The computation of the bed-load transport is based on the concept of the instantaneous bed-shear stress. The instantaneous bed-load transport rate $q_{b,t}$ is related to the instantaneous bed-shear stress, which is based on the instantaneous velocity vector (including both wave-related and current-related components; numerical intrawave approach) defined at the top of the bed load layer (i.e. small height above seabed) (Van Rijn, 2007 a). The oscillating wave-induced near bed orbital velocity due to asymmetry effects is modelled using the method of Isobe–Horikawa (1982) modified by Grasmeijer (2002).

The instantaneous bed load transport is computed as follows:

$$q_{b,t} = 0.5\,.\,\rho_s\,.\,d50\,.\,D_*^{-0.3}\,.\left(\frac{\tau_{b,cw,t}}{\rho}\right)^{0.5}\left(\frac{\max(0,\tau_{b,cw,t}-\tau_{b,cr})}{\tau_{b,cr}}\right) \qquad (2.1)$$

in which ρ_s is the sediment volumic mass, d50 is median grain size, D* is the dimensionless particle size, ρ is water volumic mass, $\tau_{b,cw,t}$ is the instantaneous bed shear stress due to combined wave and current action and $\tau_{b,cr}$ the critical bed shear stress according to Shields.

The net bedload transport vector is obtained by time-averaging of the instantaneous bed-load transport vector over a wave period T.

$$q_b = \frac{1}{T}\int q_{b,t}\;.dt \qquad (2.2)$$

Furthermore, the magnitude and direction of the bed load transport vector can be adjusted for bed slope effects.

The current-related suspended load transport consists in the transport of sediment particles by the time-averaged current velocities. It is calculated as the product of the velocity profile and the concentration profile, obtained by solving the advection-diffusion equation (Van Rijn, 2007 b) :

$$q_{s,c} = \int_a^h u\,.\,c\,.\,dz \qquad (2.3)$$

in which is the c is concentration profile, u the velocity profile; a is the reference height (top of bed-load layer), and h is total water depth.

The wave-related suspended transport is modelled following Van Rijn (2007b):

$$q_{s,w} = \gamma . \left(\frac{U_{on}^4 - U_{off}^4}{U_{on}^3 + U_{off}^3} \right) \int_a^\delta c . dz \qquad (2.4)$$

where U_{on} and U_{off} are near-bed peak orbital velocities in onshore and offshore (wave) direction, c is the time-averaged concentration, δ the thickness of suspension layer near the bed and γ a phase lag function (0.1).

Sediment transport computations are undertaken at each computational time step of the hydrodynamic module (3 seconds).

Each contribution to the total sediment transport can be separately calibrated using the coefficients f_{BED}, f_{SUS},f_{BEDW},f_{SUSW}, for the bed load transport due to currents, suspended transport due to currents, bed load transport due to waves and suspended load due to waves. In this study these coefficient were set to [1.0 1.0 1.0 0.3] respectively. A reduced value for f_{susw} was used according to suggestions in Van Rijn et al. (2004). Briere and Walstra (2006) also noted potentially unrealistic morphological evolution with a coefficient of 1 (particularly in barred beached) and used 0.3 as default value (see also Walstra et al., 2004, and Walstra et al., 2004 2008).

The sediment within the model domain was assumed to be sandy, with constant median grain size d50 of 0.3 mm. A map of sediment availability was used in simulation to reproduce non erodible areas and structures such as the Long Mac and nearshore rocky features. Sediment density was set equal to 2650 kg/m^3 and the dry bed density was set equal to 1600 kg/m^3.

2.2.4. Model Domain

The curvilinear model grids used are shown in Figure 2.2. The high resolution grid is centred on the Harbour entrance area including the Mole, Shelly Beach, and Harrington bend. The large ebb delta feature off Tairoa Heads and adjacent coastlines are also included to ensure correct representation of the complex tidal hydrodynamics (e.g. tidal jet) and properly represent the relevant the nearshore wave processes, including shoaling over the delta and wave penetration in the harbour. The wave grid used was slightly larger than the hydrodynamic grid to avoid any disturbance due to boundary effects. The hydrodynamic grid was also further refined throughout the area of interest. Grid cell sizes range from 50 m offshore to about 10-15 m near Shelly's Beach and the Long Mac.

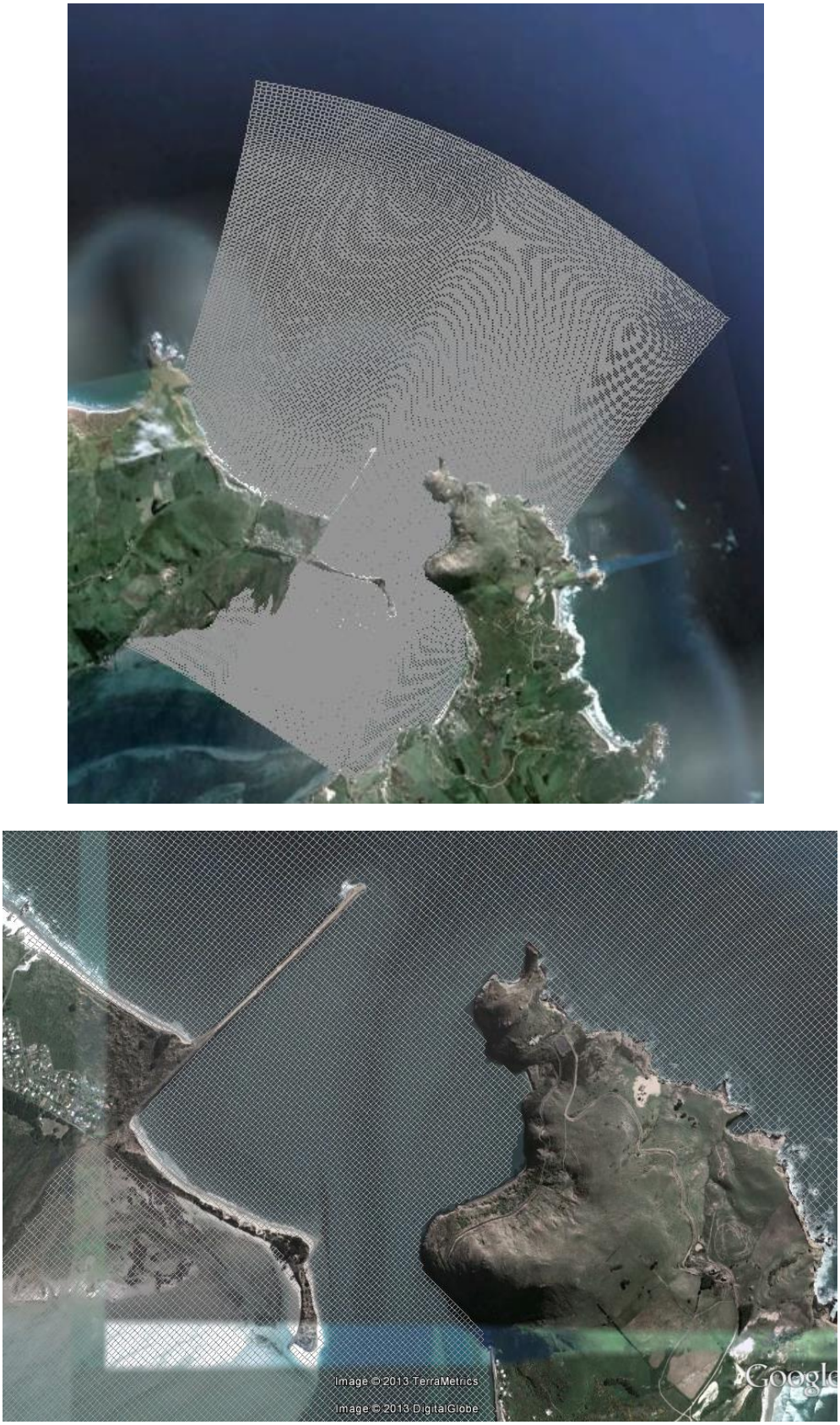

Figure 2.2 Delft3D model domain (top) and zoomed-in view near the Harbour entrance.

2.2.5. Model Setup

The key parameters used for the present study are listed in Table 2.1.

Table 2.1 Delft3D Model parameters.

Parameter	Description	Value
Wave		
BedFriction	Seabed friction formulation	collins Collins (1972)
BedFricCoef	Collins's frictions coefficient	0.015
Breaking	Depth induced breaking model	TRUE (Battjes and Janssen,1978)
BreakAlpha	Rate of dissipation	1
BreakGamma	Breaker parameter Hmax/h	0.73
WaveSetup	Wave-induced setup model	TRUE
Hydrodynamics		
Dt	Computational time step	3 s.
DryFlc	Minimum depth for drying/flooding	0.1
Vicouv	Horizontal background eddy viscosity	5
Dicouv	Horizontal background eddy diffusivity	5
Vicoww	Vertical background eddy viscosity	1.00E-06
Dicoww	Vertical background eddy diffusivity	1.00E-06
Rouwav	Model for bottom stress formulation due to combined wave and current action	#VR04# (Van Rijn et al., 2004)
BdfRou	Bedform roughness height predictor	#vanrijn07# (Van Rijn, 2007)
Sediment transport		
TraFrm	Sediment transport formulation	IFORM=-2 (Van Rijn et al.,2004)
RhoSol	Sediment density [kg/m3]	2650
SedDia	Median sediment diameter (D50) [m]	3.00E-06
CDryB	Dry bed density	1600
IniSedThick	Initial sediment layer thickness at bed [m]	space varying (5 to 0 m.)
SedThr	Minimum water depth for sediment computations [m]	0.1
Islope	Formulation of bed slope effect on bed load transport	2 (Bagnold, 1966)
AlfaBs	Streamwise bed gradient factor for bed load transport	1
AlfaBn	Transverse bed gradient factor for bed load transport	1.5
Sus	Current-related suspended sediment transport factor	1
Bed	Current-related bed-load sediment transport factor	1
SusW	Wave-related suspended sediment transport factor	0.3
BedW	Wave-related bed-load sediment transport factor	1
FWFac	Wave streaming calibration factor	0

2.3. Bathymetry data

The bathymetric dataset used for the development of the regional and local model domain bathymetries combined data from several sources including soundings and digitized nautical chart contours. In particular, a recent high resolution bathymetric survey covering the area of the Harbour entrance including the navigation channel, Shelly Beach, the Mole, the Long Mac and Harrington bend was provided by Pot Otago. Priority was given to survey data and charts contours were used in region were soundings were scarce or inexistent. Careful editing assisted with aerial photographs was employed to fill regions where no data was available, including some of the intertidal areas, and some discrete structures (e.g. subaerial section of the Long Mac). The bathymetric dataset is shown in Figure 2.3. Bathymetries of SELFE and Delft3D model domains are shown in Figure 2.4 and 2.5.

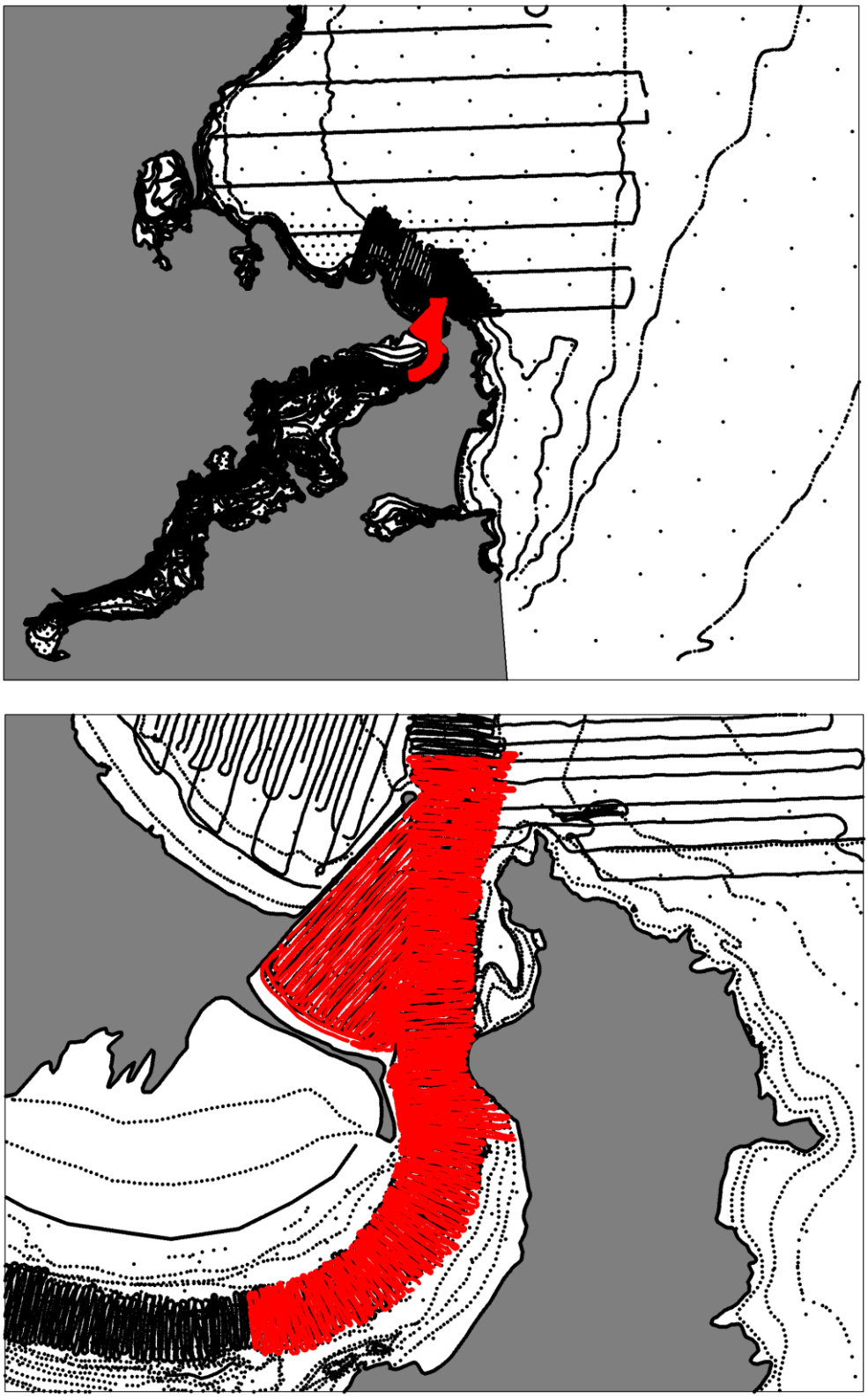

Figure 2.3 Bathymetric dataset used for model domain bathymetries. The recent survey covering the Harbour entrance is shown in red.

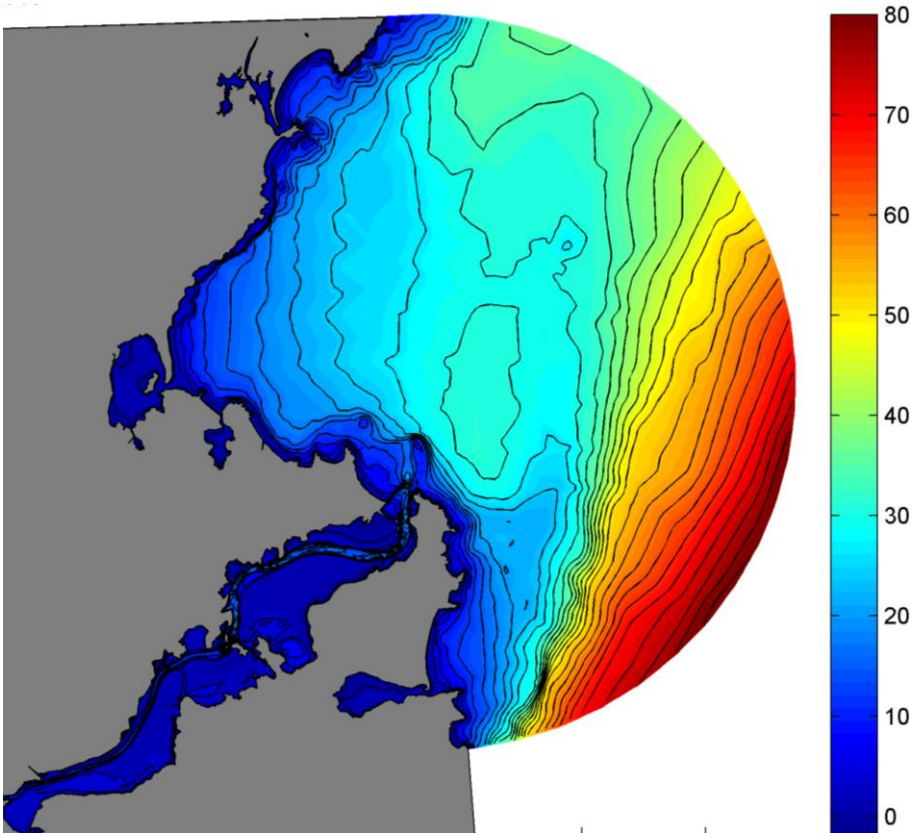

Figure 2.4 SELFE domain bathymetry.

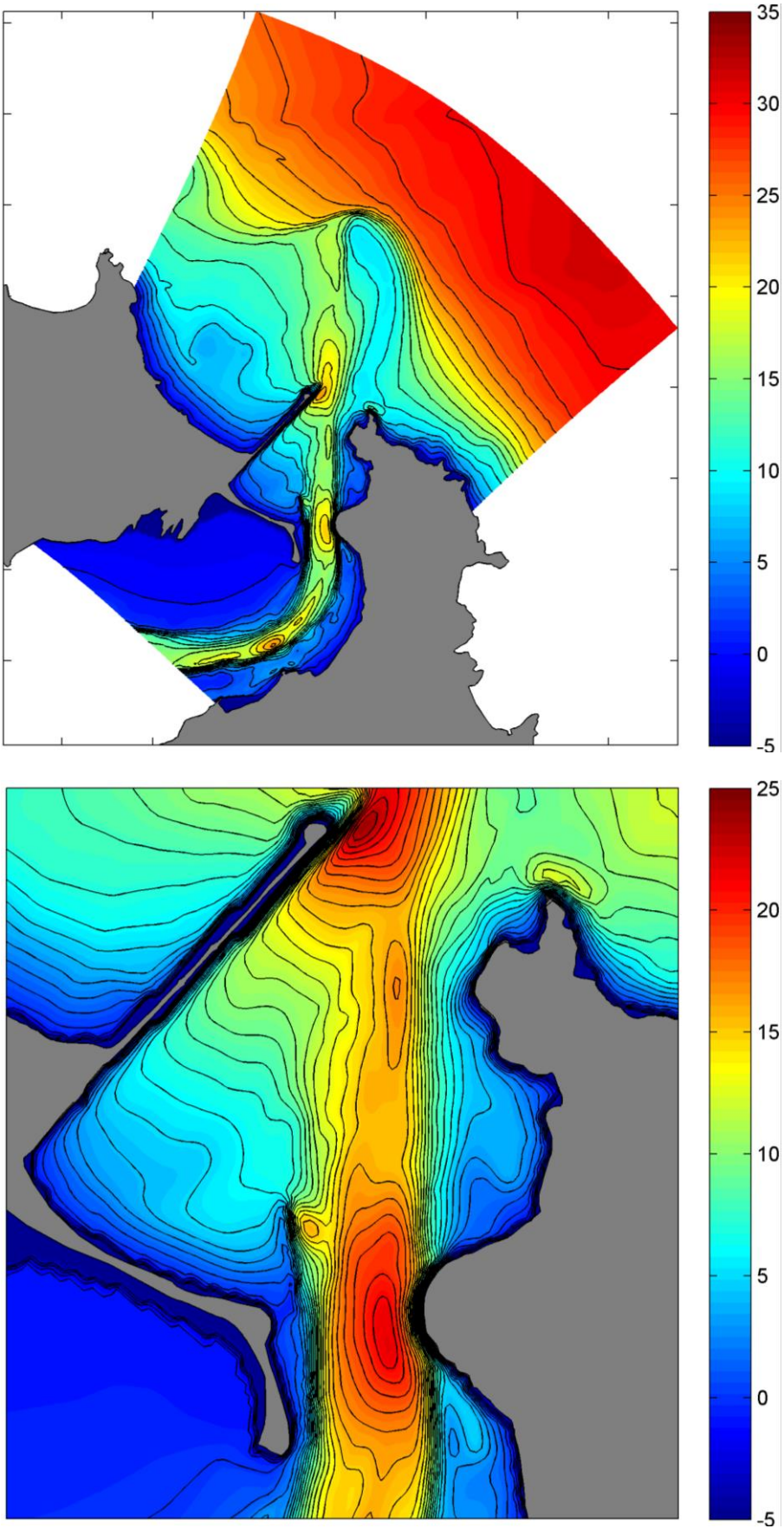

Figure 2.5 Delft3D domain bathymetry (top) and zoomed-in view of the Harbour entrance (bottom).

3. RESULTS FOR EXISTING CONDITIONS

3.1. Sensitivity analysis

To ensure robustness of the model, a qualitative sensitivity analysis was undertaken. Since we are concerned with the underlying sediment dynamics of the area rather than quantitative estimates at this stage, particular attention was given to processes that could significantly change the main flow and transport patterns developing within the Otago Harbour entrance. Based on the model setup provided in 2.2.5, without waves (i.e. tide only), some parameters were varied keeping all others the same.

3.1.1. Computational time step

As a first test, the time step of the simulation was reduced to ensure that the model was numerically stable and results were consistent for time steps within the appropriate range. The time step was reduced from 3 seconds to 1.5 seconds, thus resulting in maximum Courant numbers of ~4, which is about half of what is suggested as a limit in Deltares (2013b). No notable differences were noted and a time step of 3 seconds was retained for time efficiency reasons.

3.1.2. Friction

In Delft3D-FLOW, bottom friction can be specified following formulations of Chezy, Mannings or White-Colebrook. All these formulations require a user-input coefficient that will have direct effect on the bed shear stress estimation.

In the default setup, the bed roughness height predictor of Van Rijn (2007) is used to provide estimates of the instantaneous roughness height field (based on wave, flow and sediment parameters) in turn providing space and time-varying Chezy coefficients. This predictor provides the most sophisticated way of treating the bottom friction in Delft3D to date since instantaneous friction coefficient fields are estimated for each computational time step, which is potentially more realistic. To ensure overall consistency in results, simulations using a simpler constant Chezy or Manning coefficient, as commonly applied for coastal simulations, were undertaken for comparison with the model results with the default setup. It is noted that specifying a constant Mannings coefficient will result in friction coefficients dependent on the water depth, while a constant Chezy coefficient result in a truly constant friction coefficient throughout the model domain. Chezy coefficient of 50 and 65 and Mannings coefficient of 0.02 and 0.026 were used. They are within a range commonly used in coastal applications (e.g Deltares, 2013b Briere and Walstra, 2006) and also in the range obtained using the bed roughness predictor.

The different schemes and coefficients tested did modulate the magnitude of flows and sediment transport fluxes but main patterns were conserved with only slight variations in directions. Only the case with a constant chezy coefficient of 50 resulted in some unrealistic sediment transport fluxes on the steepest slopes of the channel. (Note that a smaller Chezy coefficient is equivalent to a larger friction). Given the overall consistency in results, the predictor of Van Rijn (2007) was conserved as default friction scheme.

3.1.3. Eddy viscosity

In coastal applications, model grids are generally too coarse and time step used too long to resolve all the turbulent scales of motions. Turbulent processes at sub-grid scale and associated energy dissipation is modelled using an eddy viscosity model. In the present study a model with constant eddy viscosity coefficient is used. The coefficient will also affect the behaviour of the flow including formation of larger eddies developing at grid scale. More simply, it can be seen as a measure of how viscous or "thick" the seawater mass will be as it propagates over the bathymetry. The value of the horizontal eddy viscosity coefficient depends on the flow and the grid size used in the simulation. The grid used here is relatively detailed and will resolve much of the details of the flow and a typical range for the coefficient value is 1 to 10 m^2/s. (Deltares, 2013b). Coefficients of 1,5, and 10 were tested.

Snapshots of circulations within the Harbour entrance with different eddy viscosity coefficients are shown in Figures 3.1 and 3.2 for outgoing and incoming tides. During an outgoing tide, the ebb flow spreads and slightly weakens past the Long Mac seaward tip and the flow portion that veering westwards tend to drive a return easterly flow along Shelly beach. The eddy viscosity coefficient has an effect on the flow "spreading" and in turn modulates the magnitude of the return flow along Shelly Beach. A smaller coefficient results in more water veering westwards and a stronger return flow along Shelly Beach. A distinct eddy is visible just west of the Long Mac for the simulation with an eddy viscosity of 1 m^2/s. As the tide comes in, a water level gradient is expected to develop along Shelly Beach, relative to the channel level. This drives a longshore easterly flow along the beach that accelerates over the Long Mac. Consistent patterns are reproduced for the different eddy viscosities with slight variations in flow direction and magnitudes. The main difference is a return flow that develops along the Mole for a coefficient of 1 m^2/s that is not reproduced in the other cases.

The difference in circulation and eddy formation is clearly relevant with respect to the morphodynamic response of the area. However, these processes are hard to verify without field information. The central range value of 5 m^2/s was conserved.

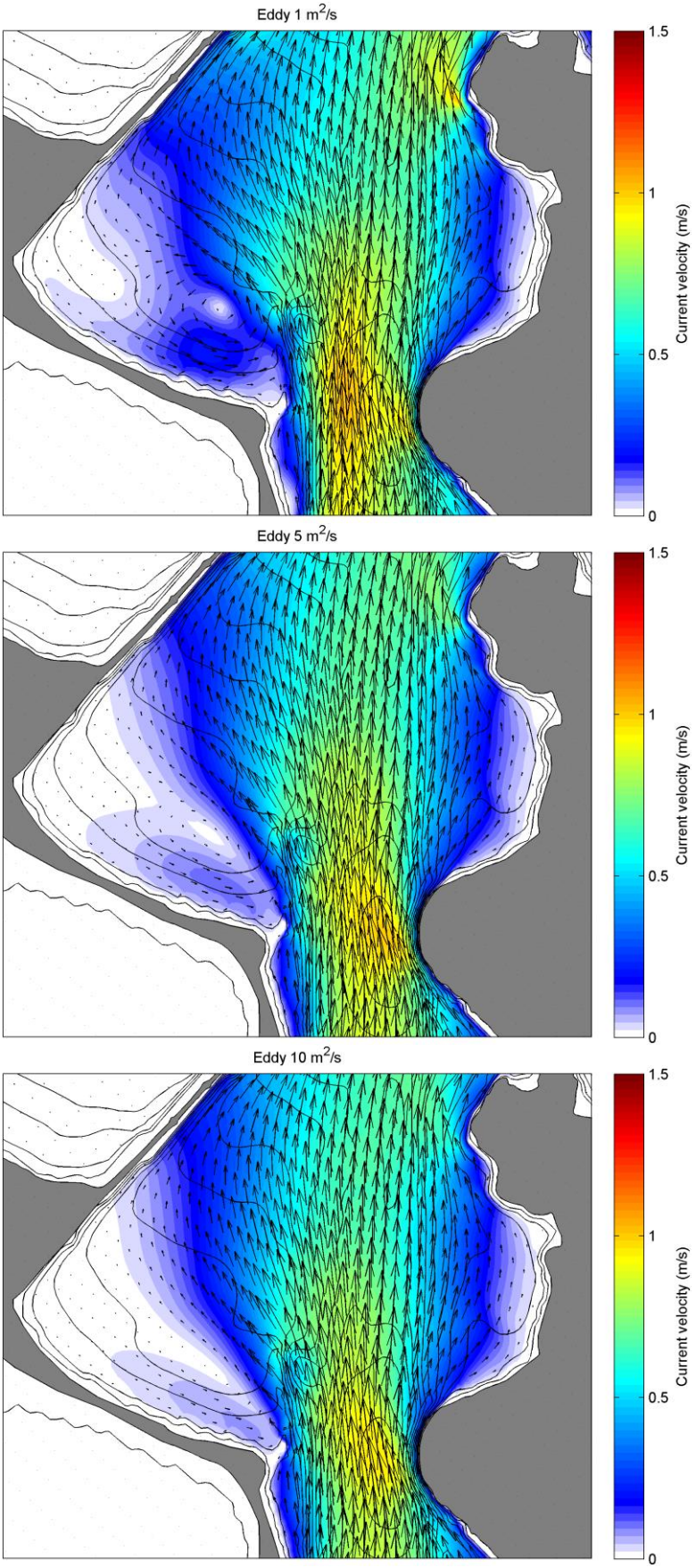

Figure 3.1 Snapshot of modelled flow fields with different eddy viscosity coefficients at an outgoing tide.

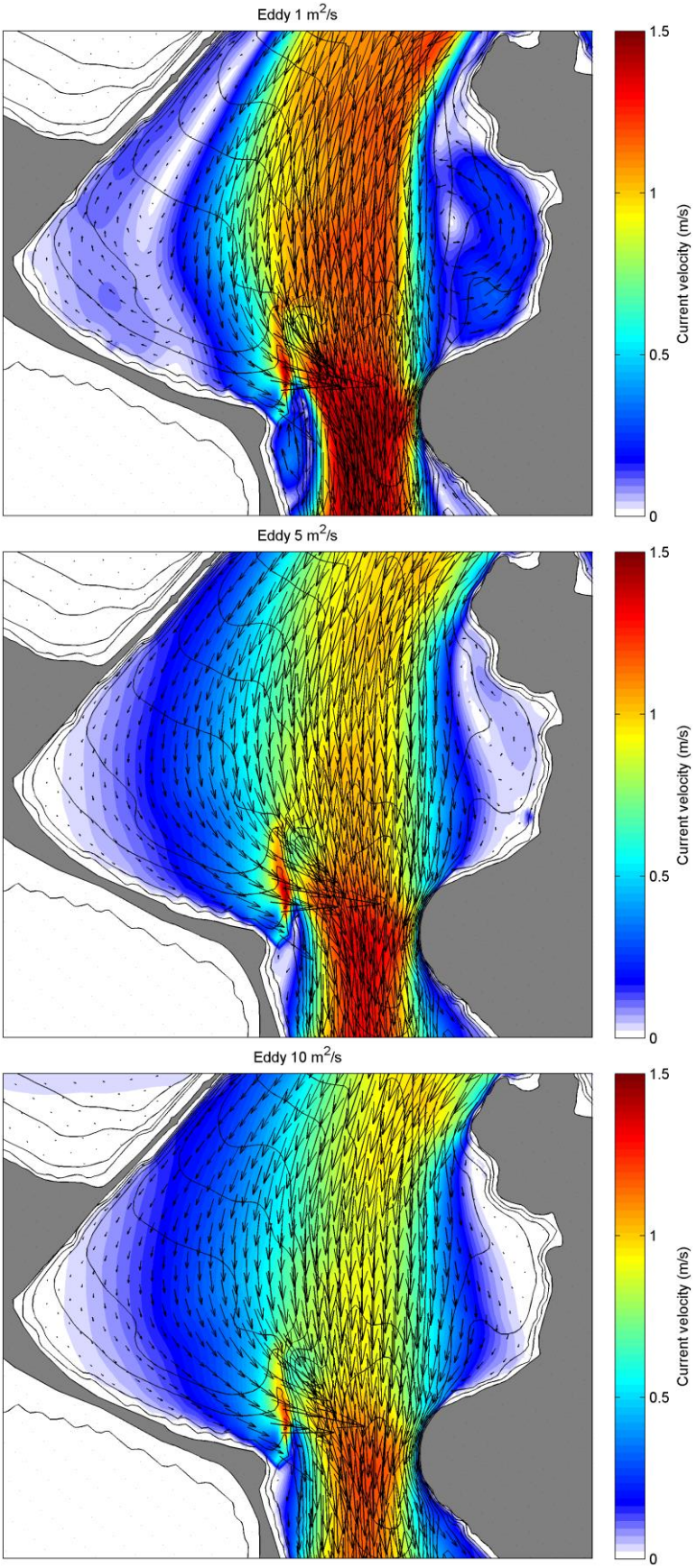

Figure 3.2 Snapshot of modelled flow fields with different eddy viscosity coefficients at an incoming tide.

3.1.4. Grain size

The specified median grain *d50* is a key parameter in the computations of the bed roughness field and sediment transport fluxes, particularly the bed-load fraction. The default value of 300 microns used in the basic setup was supplemented by simulations using *d50* of 200 and 400 microns.

The roughness predictor appears to be relatively stable with respect to the user-input *d50* and derived friction coefficients are relatively consistent. An example at a given time step is given in Figure 3.3. This will modulate flow magnitudes but is not expected to induce any significant variations in flow patterns. Predicted transport fluxes for the different grain sizes are compared in Figure 3.4 and 3.5. Difference in magnitude are clearly visible however underlying patterns are quasi identical. Given the absence of field information these flux magnitudes can hardly be calibrated. This is not critical at this stage since we are more concerned with general sediment patterns rather than quantitative estimates.

3.1.5. Conclusion

Based on the brief sensitivity analysis, it is identified that the eddy coefficient will potentially have the most effects in the predicted flows and transport patterns. However, results are still relatively consistent and it is expected that the default model setup will allow identifying the key processes of the area. Variations related to friction and grain size are not significant at this stage but are identified as important parameters for future applications when a more quantitative approach is required.

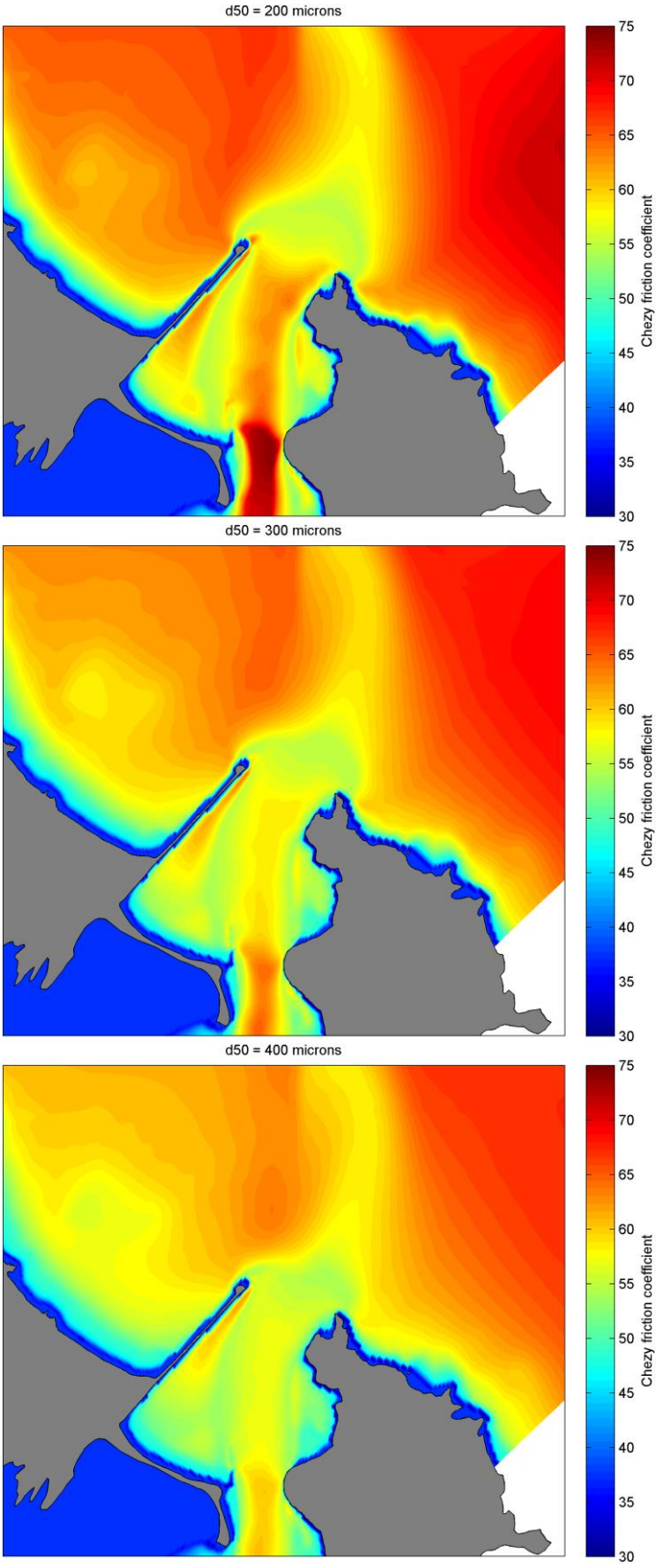

Figure 3.3 Predicted Chezy friction coefficients using the bed roughness predictor of Van Rijn (2007) for different median grain sizes, at same time step.

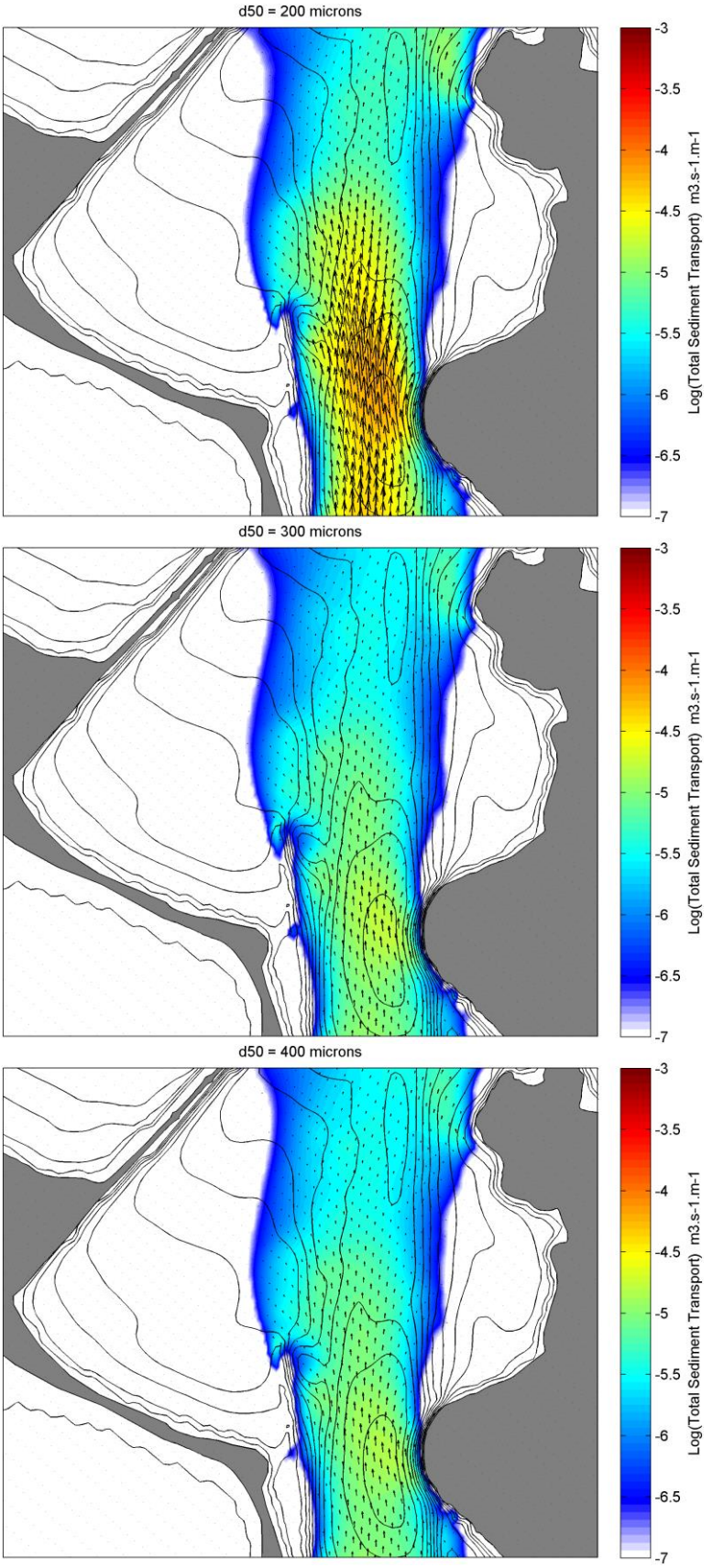

Figure 3.4 Snapshot of modelled total sediment transport fluxes with different median grain sizes at an outgoing tide.

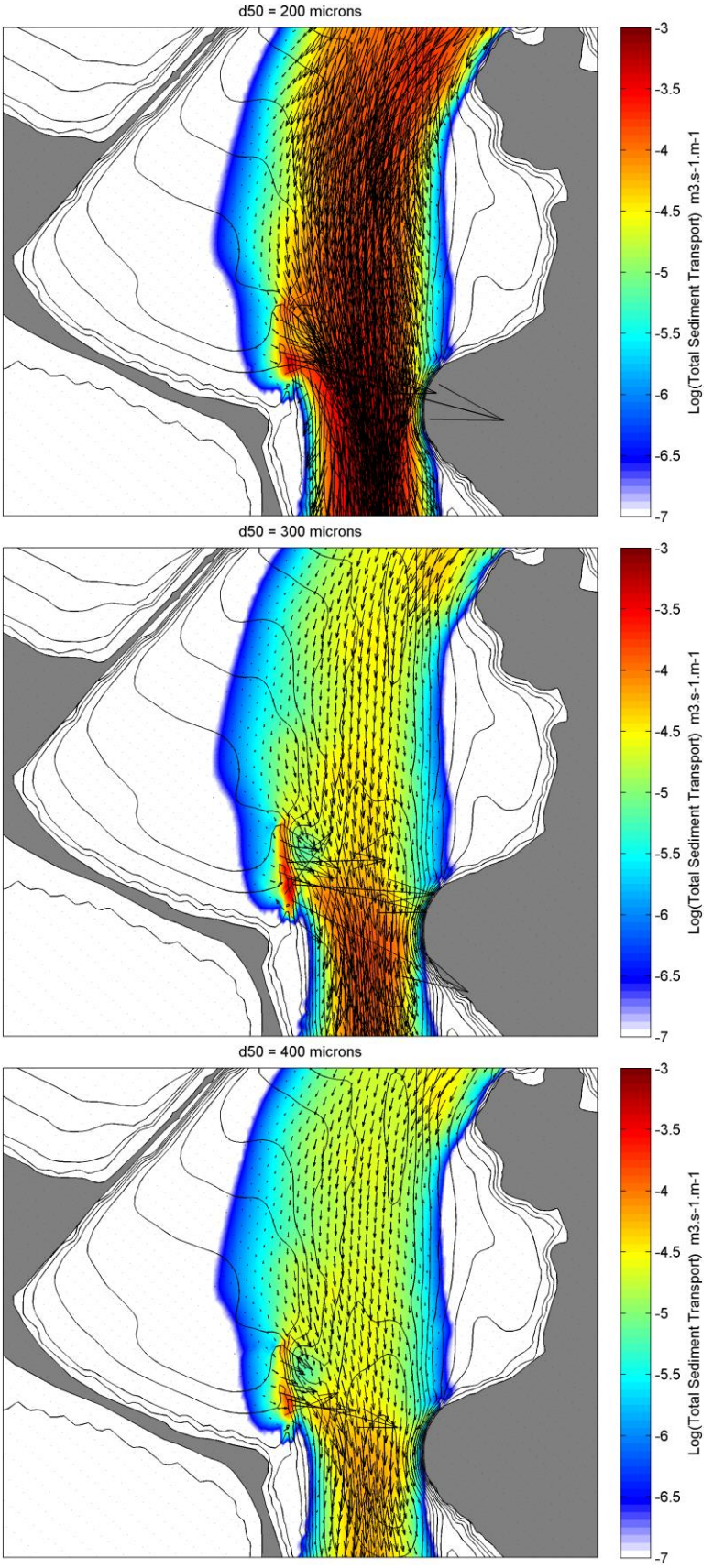

Figure 3.5 Snapshot of modelled total sediment transport fluxes with different median grain sizes at an incoming tide.

3.2. Scenario results

3.2.1. Events simulated

For all events, the simulation period covered several spring tidal cycles (16/04/2011 - 20/04/2011) to capture some of the most critical ambient tidal flows expected to occur in the entrance region. The model was run without wave action to get a picture of the underlying hydrodynamics, and for different idealized wave events. The idealized events aimed at covering the range of wave conditions expected at the site, with a particular interest on cases when wave energy penetration within the entrance area and potential for sediment transport is important. Wave events were selected based on joint probabilities available from a previous study (MetOcean Solutions Ltd., 2011). Events are summarized in Table 3.2. They include large swells from the southeast and northeast, and both high energy swell and low energy sea waves from the north.

To identify the key transport pathways within the entrance region, the simulation outputs were averaged over the incoming and outgoing tidal phases, and over the complete tidal cycles. Incoming and outgoing phases were defined based on the water level at the mouth. These averaged outputs are supplemented by particular model snapshot.

Table 3.1 Simulated events

Simulations	Hs (m)	Tp (s)	Dp (deg. true)
SE event	3	14	135
NE event	3	10	45
N event swell	2	14	0
N event sea	1	8	0

3.2.2. Tidal circulation and sediment transport

Snapshots of peak ebb and flood flows are shown in Figures 3.6. During an outgoing tide, strong water level gradients due to the water mass retained within the Harbour drive a clear ebb jet. The flow is constricted by the Harbour mouth and slightly widens past the seaward tip of the Long Mac. The jet extends well offshore, following the channel along the large submerged delta bar. During a flood tide state, opposed water level gradients drive strong southwards flows within the channel as the Harbour fills. It is evident that the entrance region enclosed by the Mole fills in faster than the volume that can enter the Harbour and as a result a water level gradient develops along Shelly Beach. This drives an easterly-directed flow along the beach that accelerates over the Long Mac as it meets the constricted channel flows.

To serve as a reference point for future comparison with cases with wave action, incoming, outgoing and full-cycle averaged flows and transport fields were processed for the tide-only simulation (Figs. 3.7 to 3.9). For incoming tides, the mean flow pattern appears as a smoothed version of the peak flood flow shown in Figure 3.6. There is a distinct alonghsore current along the eastern half of Shelly Beach, which accelerates over the

Long Mac before meeting with the channel flood flows constricted by the mouth.

This process is very significant with respect to potential sediment recirculation in the Harbour. Sediment transport vectors over the Long Mac are clearly directed eastwards and to the channel and tend to direct sediment towards the area of increased ambient southwards transport developing throughout the mouth due stronger constricted flow velocities. However it is noted that the transport further west from the structure rapidly reduces. This means that the tide-driven alongshore flow is not of sufficient strength to mobilize sediments from Shelly Beach.

Outgoing tidal flows and transport are shown in Figure 3.8. The ebb jet clearly dominates the flow and transport regime at outgoing tide phases. The Long Mac tends to slightly constrain the local jet, and a slight spreading of the flow is visible past its seaward tip. The full cycle mean maps (Fig. 3.9) reproduce the 2 main features discussed above with a net northwards flow within the channel and a net east-southeast component along Shelly Beach and over the Long Mac.

3.2.3. Wave-driven circulation and sediment transport

The tidal processes identified in 3.2.2 will be modulated by the wave-driven currents and water level setups when wave energy penetrates the entrance region.

Mean significant wave heights for the different wave events simulated are shown in Figures 3.10 and 3.11. For the southeast and northeast events, the wave energy tends to predominantly reach the western half of Shelly Beach (Fig. 3.10). A secondary region of larger height is noted in the bay east of the channel that receives wave energy refracted by the channel margin. Larger heights are experienced for the northeast event with significant wave heights of 1.5-1.8 m along the beach. The northerly events result in a more homogeneous height distribution along the beach. A distinct band of larger height reaching the centre of the beach develops for the long period swell event. Note that the local bathymetry showing remnant of the dump mounds will further focus incident wave energy. The Long Mac structure is seen to provide some limited sheltering from incident waves during the high energy northeast and north events along the eastern end of Shelly Beach. Some mild focusing of wave heights can be identified on the seaward tip of the structure.

Mean incoming flows are shown in Figure 3.12 for the southeast and northeast events. The underlying tidal flow patterns are mostly conserved but some wave-driven flows develop along the beach. Flow velocities in the Long Mac vicinity are slightly stronger for the northeast case, which is due to the larger transmitted wave energy and a relative increase in the local water level gradients. More significant differences relative to the tide-only case are visible in the mean incoming sediment transport maps (Figure 3.13). The wave action results in an onshore transport flux at Shelly Beach and mobilization of the sediment along the beach. This is the most distinct for the northeast event for which ambient wave energy is larger. Easterly transport fluxes are predicted in the vicinity of the Long Mac, with stronger magnitude for the northeast event.

The mean incoming flows and transport for the northerly events are compared in Figures 3.14 and 3.15. For the swell event, the wave energy forces an alongshore westerly flow along the western half of Shelly Beach, eventually being redirected (clockwise) along the Mole. Easterly sediment transport fluxes are reproduced in the vicinity of the Long Mac however it is noted that the transport magnitude for the northerly swell event is visibly less than that for the northeast event (Fig. 3.13). This is likely due to a different water level gradient distribution along the beach during the northerly swell event, for which the more central position of transmitted wave energy and associated water level setup will force some of the incoming water mass west and along the Mole rather than east towards the Long Mac and channel. As expected, the wave-driven sediment transport is much less for the low energy sea wave event.

Results for the outgoing tide phases are shown in Figures 3.16 to 3.19. The mean outgoing flow field for the southeast and northeast events (Fig. 3.16) indicates that the circulation is still dominated by the ebb jet. For the northeast event, a wave-driven return flow develops along the western half of Shelly Beach and corresponds in the sediment transport map (Fig. 3.17) to a distinct westerly longshore transport vector. This feature was not present in at incoming tide phases. This is likely due to the ambient tidal water levels gradients working against such flow at during incoming tides (see water levels during peak flood flows Fig. 3.6). Comparison of mean wave heights during incoming and outgoing tide phases (Fig. 3.24) suggest that this may also be related to slight shift of location of the band of highest wave energy along the beach. Refraction of the incident wave filed will be modified by the different water level and ambient flow fields which will result in slightly different patterns within the entrance. It is noted that the incident wave filed is subject to intense refraction processes off the entrance due to the submerged ebb delta bar (see Metocean Solution Ltd., 2013). In that case the band of higher wave energy is slightly shifted east thus forcing a return flow along the Mole. This alonghsore feature tends to dominate the sediment transport regime along the beach for the northeast event. Some wave-induced transport develops along the eastern half of Shelly Beach and in the vicinity of the Long Mac, which was not observed for the tide-only case or even the south east case. It is however an order of magnitude weaker than west of the beach. Patterns are relatively consistent but one to two orders of magnitude weaker for the southeast case, due to the less energetic ambient wave forcing.

Mean summary maps for the northerly events for outgoing tide phases are provided in Figures 3.18 and 3.19. The main wave-driven flow and transport patterns along Shelly Beach are mostly conserved relative to the incoming tide phases (Figs. 3.12 and 3.13). However, the magnitude of the longshore westerly transport along the western half of the beach is clearly enhanced for the swell event (left). This is again likely due to more favourable ambient water level gradients. A slight shift of the transmitted wave energy band towards the centre of the beach is again evident for the outgoing phases (Fig. 3.25), which seems to force the flow more to the west. A small area of wave-induced transport is visible over the tip of the Long Mac due to local wave focusing by the structure. The lower energy sea wave event results in less intense transport, limited to the intertidal region of the beach and predominantly directed offshore.

It is noted that for both northerly events and the northeast event, for both incoming and outgoing phases, some sediment is mobilized on the small bay east of the channel mouth, although generally with an order of magnitude less than along Shelly Beach.

The flow and sediment transport fields averaged over the complete tidal cycles are provided in Figures 3.20 to 3.23. Generally they reproduce and combine processes identified at incoming and outgoing phases thus providing summary maps. Features reproduced for all cases include the wave-driven onshore transport seaward of Shelly Beach, with variations in direction in magnitudes, and a net northwards (outgoing) flow and sediment transport component within the channel. The onshore transport at Shelly Beach and over the disposal ground clearly coincides with the region of transmitted wave energy. This indicates that the wave-driven transport due to wave asymmetry effects as wave propagates shoreward possibly further shoaling over the remnant mound is an important process for the area. This will result in a progressive shoreward migration of the dumped sediments, providing direct sediment supply to the Shelly Beach system. A comparison of bathymetric contours from the older data available, and that from the latest survey shows a clear onshore translation of the depth contours over an area coinciding with the general position of the wave energy band (Fig. 3.26).

More locally, some contrasting net flow patterns are obtained for the southeast and northeast events (Fig. 3.20). For the northeast event, the more significant wave energy penetration and associated wave-driven setup and flows strengthen the easterly tidal currents flowing towards the Long Mac and channel along the eastern half of Shelly Beach and drive a return flow towards the Mole, along the western part of the beach. This results in net sediment transport vectors pointing to the channel in the vicinity of the Long Mac, and longhsore sediment transport fluxes towards Shelly Beach western corner further to the west. In contrast, mean flows for the southeast case are overall very similar to the tide-only mean flow field (Fig. 3.9). With respect to sediment transport in the Long Mac vicinity, the easterly vectors are reproduced but magnitudes are smaller than for the northeast case and wave-induced transport along the beach is not significant.

The energetic northerly swell forcing (Fig. 3.22, left) disturbs the underlying net tidal flows developing seaward and along Shelly Beach, i.e. first southwards then veering eastwards and towards the channel. Wave-driven flow and water level setup result in a longshore flow towards Shelly Beach western corner and along the Mole. This “evacuation” of water through a different path reduces the flow magnitude along the Shelly Beach eastern half and over the Long Mac (relative to the tide-only case and northeast event). Interestingly, the flow component along the Mole appears to merge with incoming south-southeastwards flows further off Shelly Beach, eventually meeting with the easterly flows in the vicinity of the Long Mac. The wave-induced flow towards the Mole mobilizes sediment with distinct net northwesterly longshore fluxes. Although not obvious in the total transport maps it is expected that some of that sediment be eventually redirected in the channel vicinity through the return flow pattern off Shelly beach identified above. This return pattern is visible in net suspended transport fluxes for the north swell event (Fig. 3.27), although an order of magnitude less than the total transport fluxes shown. This signal is masked

by the bed load transport that obviously dominates the sediment transport regime. Easterly-directed sediment transport vectors due to flow acceleration over the Long Mac are again reproduced for both cases over the Long Mac. However, magnitudes are visibly smaller than for the northeast event, even for the high energy event. This is likely due to the development of a stronger return along the Mole providing a degree of "relaxation" to the flow forcing in the vicinity of Long Mac.

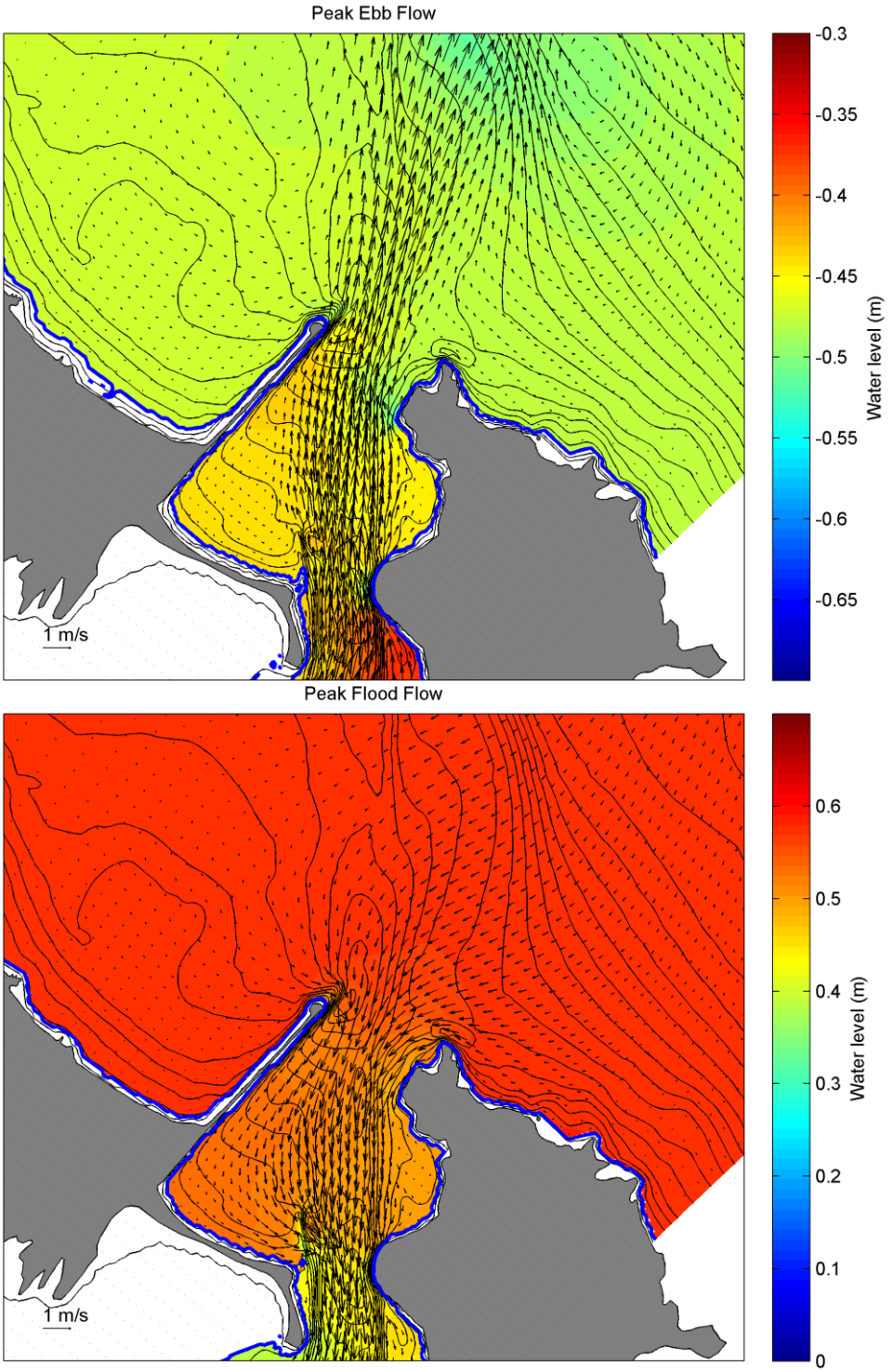

Figure 3.6 Snapshot of peak ebb (top) and flood (bottom) water levels and flow fields for the case without wave action.

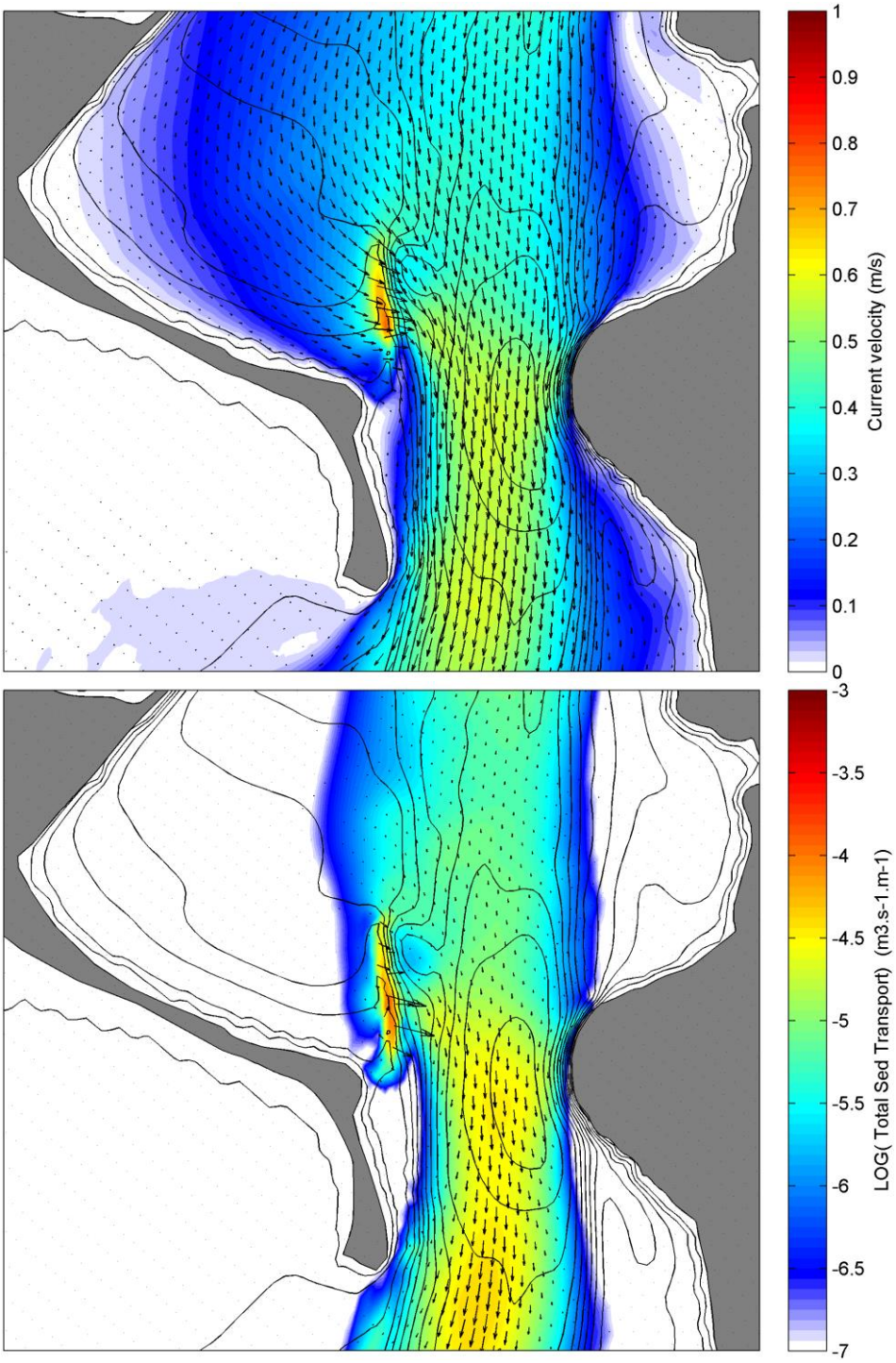

Figure 3.7 Mean flow field (top) and total sediment transport fluxes (bottom) for incoming tide phases, for the case without wave action.

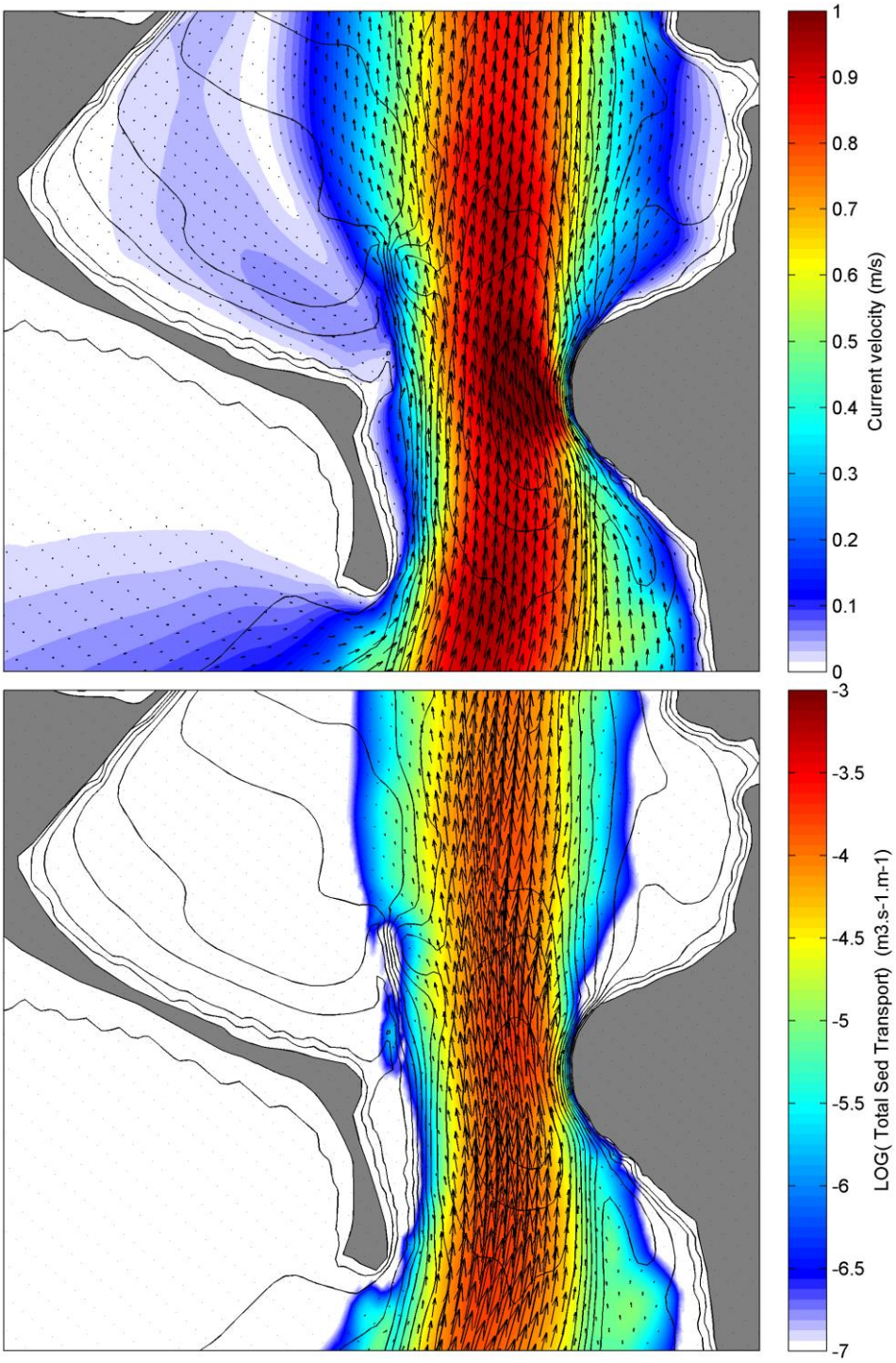

Figure 3.8 Mean flow field (top) and total sediment transport fluxes (bottom) for outgoing tide phases, for the case without wave action.

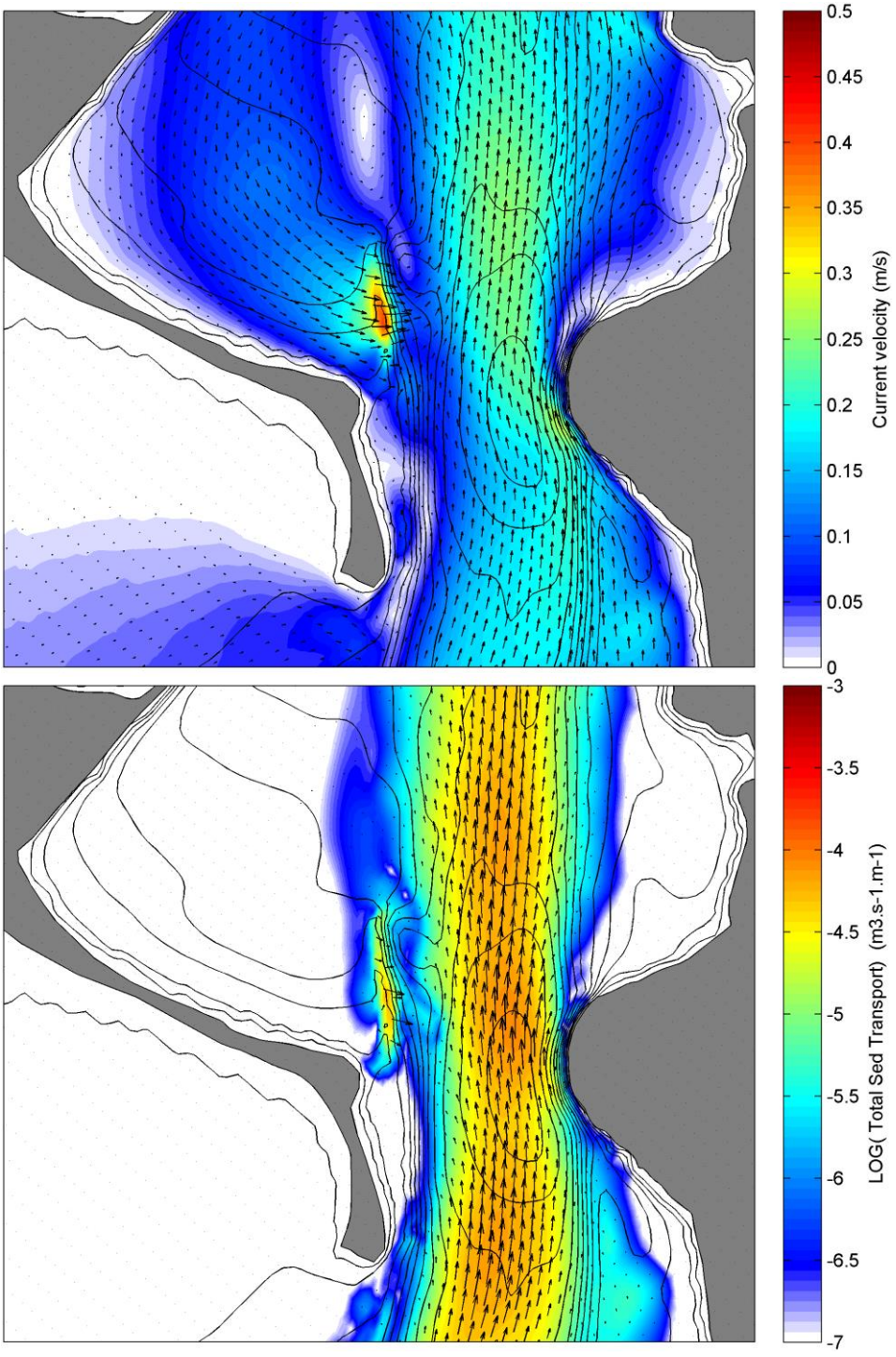

Figure 3.9 Mean flow field (top) and total sediment transport fluxes (bottom) for the full tidal cycles, for the case without wave action.

Hs=3m, Dir=135 deg., Tp=14 s.

Hs=3m, Dir=45 deg., Tp=10 s.

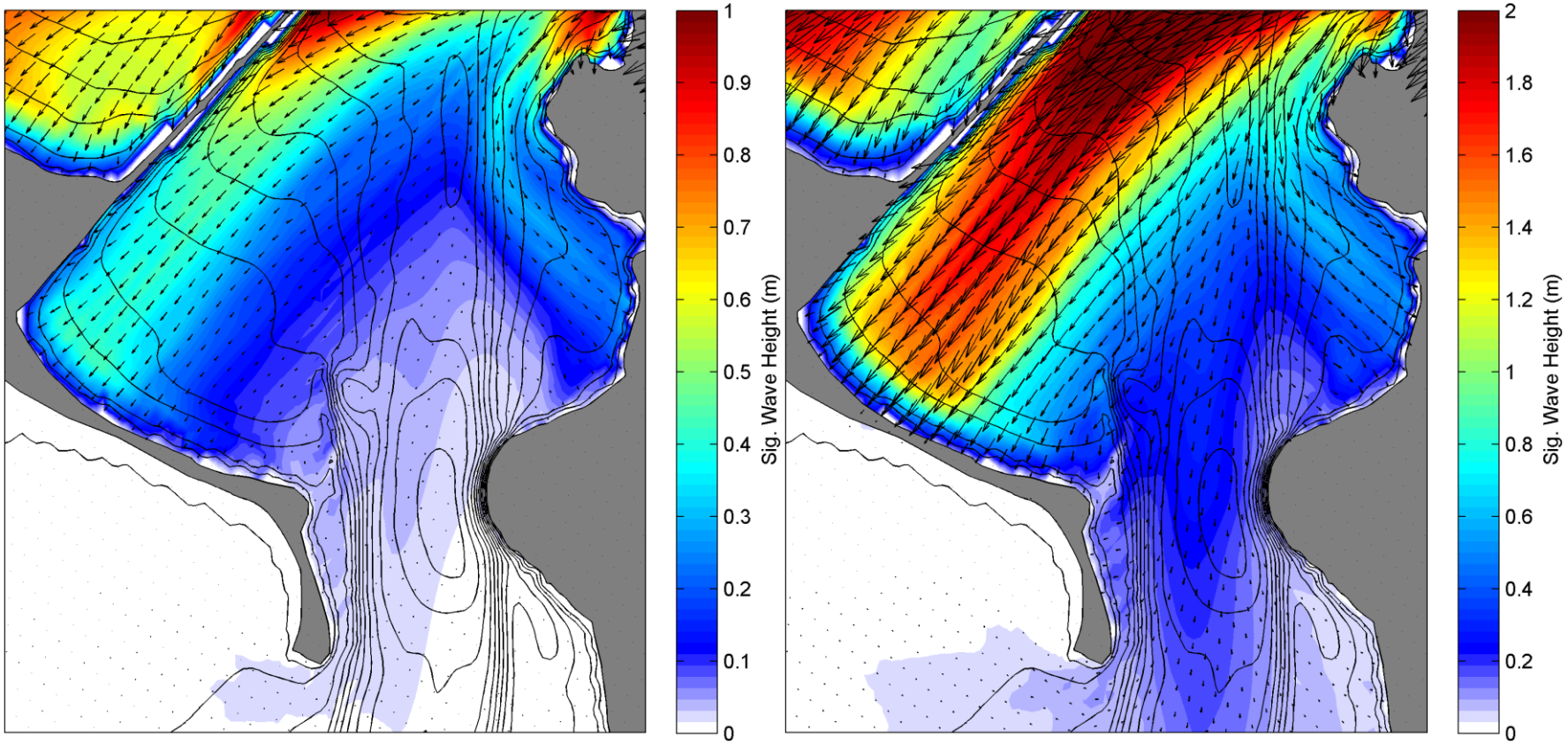

Figure 3.10 Mean significant wave heights within the entrance region for high energy southeast (left) and northeast (right) wave events (southeast event: Hs=3m, Dir=135 deg., Tp=14 s.; northeast event: Hs=3m, Dir=45 deg., Tp=10 s.). Note the different color scales for the 2 events

Hs=2m, Dir=0 deg., Tp=14 s.

Hs=1m, Dir=0 deg., Tp=8 s.

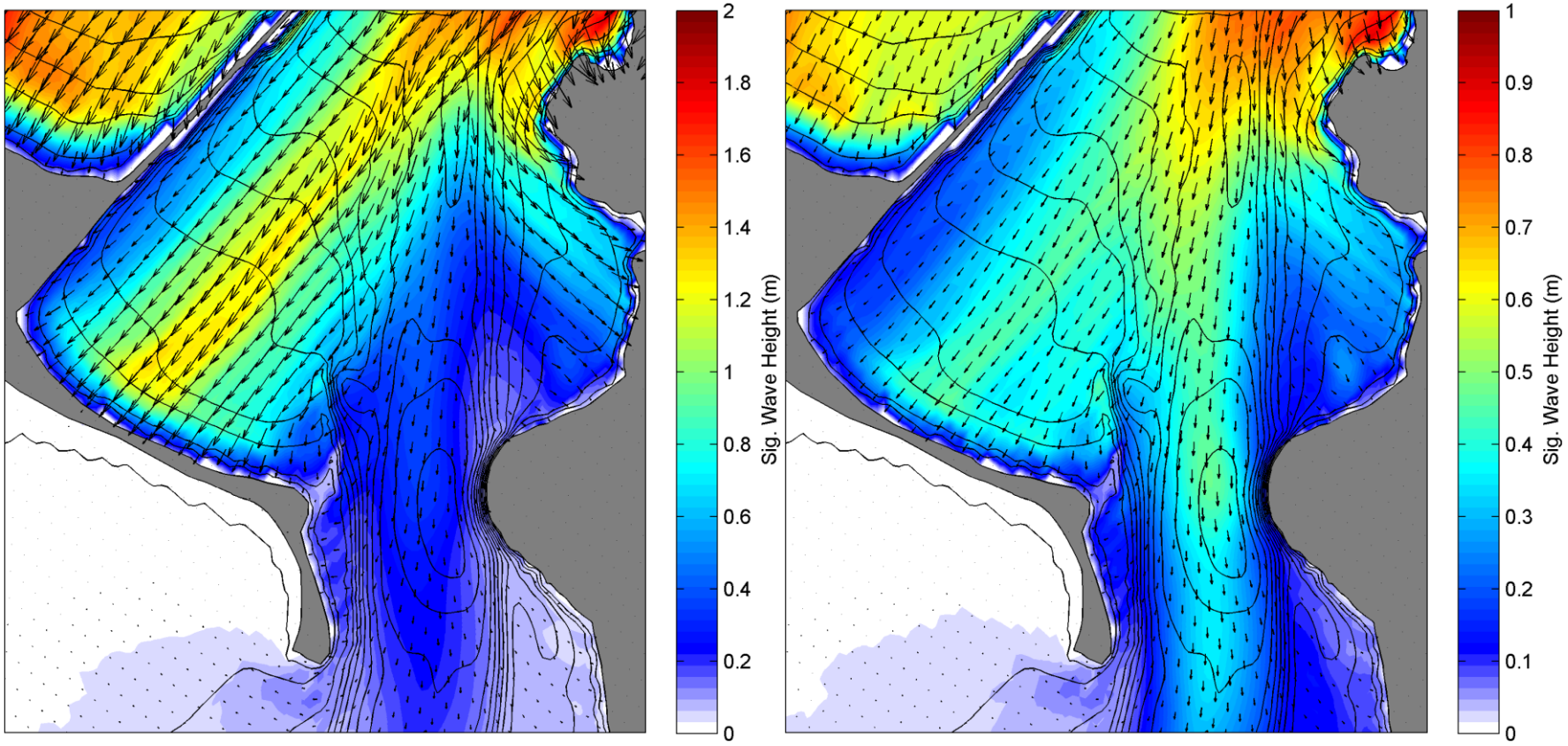

Figure 3.11 Mean significant wave heights within the entrance region for high energy north swell waves (left) and low energy sea waves (north swell event: Hs=2m, Dir=0 deg., Tp=14 s.; north sea event: Hs=1m, Dir=0 deg., Tp=8 s.). Note the different color scales for the 2 events.